AGU PUBLICATIONS

JGR

Journal of Geophysical Research: Atmospheres

RESEARCH ARTICLE
10.1002/2016JD026225

Key Points:
- We make recommendations for a self-consistent representation of lightning NO_x simulation
- Observation-based preconvection lightning NO_x profiles can be used directly with WRF convective transport
- Convective redistribution is a more important factor than preconvection Lightning NO_x profile selection

Correspondence to:
Y. Wang,
yuhang.wang@eas.gatech.edu

Citation:
Luo, C., Y. Wang, and W. J. Koshak (2017), Development of a self-consistent lightning NO_x simulation in large-scale 3-D models, *J. Geophys. Res. Atmos.*, *122*, doi:10.1002/2016JD026225.

Received 20 NOV 2016
Accepted 10 FEB 2017
Accepted article online 14 FEB 2017

Development of a self-consistent lightning NO_x simulation in large-scale 3-D models

Chao Luo[1], Yuhang Wang[1], and William J. Koshak[2]

[1]Georgia Institute of Technology, Atlanta, Georgia, USA, [2]NASA-Marshall Space Flight Center, National Space Science and Technology Center, Huntsville, Alabama, USA

Abstract We seek to develop a self-consistent representation of lightning NO_x (LNO_x) simulation in a large-scale 3-D model. Lightning flash rates are parameterized functions of meteorological variables related to convection. We examine a suite of such variables and find that convective available potential energy and cloud top height give the best estimates compared to July 2010 observations from ground-based lightning observation networks. Previous models often use lightning NO_x vertical profiles derived from cloud-resolving model simulations. An implicit assumption of such an approach is that the postconvection lightning NO_x vertical distribution is the same for all deep convection, regardless of geographic location, time of year, or meteorological environment. Detailed observations of the lightning channel segment altitude distribution derived from the NASA Lightning Nitrogen Oxides Model can be used to obtain the LNO_x emission profile. Coupling such a profile with model convective transport leads to a more self-consistent lightning distribution compared to using prescribed postconvection profiles. We find that convective redistribution appears to be a more important factor than preconvection LNO_x profile selection, providing another reason for linking the strength of convective transport to LNO_x distribution.

Plain Language Summary Lightning is a major source of nitrogen oxides ($NO_x = NO + NO_2$) and can significantly affect the chemistry and atmospheric composition in the upper troposphere. We develop a self-consistent representation of lightning NO_x (LNO_x) simulation in a regional 3-D model. After testing a large suite of meteorological and microphysical variables related to convection, we find that the parameterization using convective available potential energy and cloud top height gives the best flash rate estimates compared to July 2010 observations from ground-based lightning observation networks over the United States. With the advancements of meteorological models, we show that observation-based preconvection LNO_x emission profiles can be directly applied in 3-D model simulations. The redistribution of LNO_x by simulated convective transport produces satisfactory results compared to available in situ observations. The effect of convective redistribution is found to be larger than the prescribed preconvection LNO_x profile.

1. Introduction

Lightning is a major source of nitrogen oxides ($NO_x = NO + NO_2$) in the upper troposphere [e.g., *Lamarque et al.*, 1996; *Allen et al.*, 2000]. Lightning NO_x (LNO_x) exerts a disproportionally large influence on upper tropospheric chemistry due in part to longer lifetimes of NO_x in the middle and upper troposphere than in the boundary layer. Previous studies showed that the estimates of the magnitude of the LNO_x source and its vertical and spatial distributions are all important in model simulations [e.g., *Stockwell et al.*, 1999; *Labrador et al.*, 2004; *Choi et al.*, 2005; *Schumann and Huntrieser*, 2007; *Hudman et al.*, 2007; *Tost et al.*, 2007; *Zhao et al.*, 2009; *Martini et al.*, 2011].

Lightning takes place during convection. In order to obtain self-consistent LNO_x simulations in a large-scale 3-D model, the LNO_x source is often parameterized as a function of meteorological variables sensitive to convection [e.g., *Price and Rind*, 1992; *Wang et al.*, 1998b; *Allen and Pickering*, 2002; *Choi et al.*, 2005; *Zhao et al.*, 2009]. Many field observations [e,g., *Williams and Lhermitte*, 1983; *Dye et al.*, 1989; *Rutledge et al.*, 1992; *Carey and Rutledge*, 1996; *Petersen et al.*, 1996, 1999; *Deierling and Petersen*, 2008; *Finney et al.*, 2014; *Carey et al.*, 2016] suggest that updraft is a key process for charge separation within a thunderstorm because of its effects on graupel and ice crystals and their collisions. Cloud-resolving models [e.g., *Pickering et al.*, 1998; *Barthe and Barth*, 2008; *Barthe et al.*, 2010; *Ott et al.*, 2010] can be applied to simulate the detailed

microphysical processes and their effects on LNO_x in a self-consistent manner. However, regional- and global-scale models often do not have the necessary resolutions to do so. Bulk parameterizations using meteorological variables such as cloud top height (CTOP), upward cloud mass flux (UMF), convective precipitation rate (CPR), and convective available potential energy (CAPE) are often used to estimate the spatiotemporal distribution of lightning flash rates [e.g., *Price and Rind*, 1992; *Allen and Pickering*, 2002; *Choi et al*., 2005; *Wong et al*., 2013].

Due largely to the need for severe thunderstorm detection and warning, real-time lightning detection systems, such as the National Lightning Detection Network (NLDN) and North Alabama Lightning Mapping Array (NALMA) [e.g., *Cummins and Murphy*, 2009; *Koshak et al*., 2004], have been deployed to determine the location and strength of lightning flashes. More recently, the Earth Networks Total Lightning Network (ENTLN) was deployed (http://www.earthnetworks.com/). We will make use of these observations in order improve the model parameterization of LNO_x.

In large-scale 3-D models, LNO_x vertical distributions are prescribed in the model. *Pickering et al*. [1998] recommended a C-shaped profile for use for LNO_x distribution over land in midlatitudes, in which the major portion of LNO_x is distributed in the upper troposphere. In comparison, the updated LNO_x profile in a more recent cloud-resolving model study by *Ott et al*. [2010] places a major portion of LNO_x in the middle troposphere. On the other hand, the observations from the NLDN and the NALMA can be used to estimate the LNO_x distribution directly using the NASA Lightning Nitrogen Oxides Model (LNOM) [*Koshak et al*., 2014]. However, there is a subtle but critical difference between computed [*Pickering et al*., 1998; *Ott et al*., 2010] and observation-based LNO_x distributions. Cloud-resolving model estimated (postconvection) LNO_x profiles are simulated after LNO_x is redistributed by convective transport, while LNOM observation-based (preconvection) LNO_x profiles are made before the redistribution of convective transport. Therefore, the preconvection and postconvection profiles cannot be compared directly and should be used appropriately in model simulations.

Since cloud-resolving models are computationally too expensive to be applied over large regions, large-scale (regional or global) models are still the primary tools for understanding regional- or global-scale chemistry, transport, and circulations. If not explicitly stated, "model" in this paper refers to a large-scale model. It is desirable to use lightning observations to directly constrain the model LNO_x simulations. The difficulty is that the location of simulated convection can be misplaced in meteorological simulations compared to the observations, leading to lightning that occur in regions without deep convection in the model. *Kaynak et al*. [2008], for example, used simulated cloud data to distribute LNO_x vertically, but the lightning frequency and location data are from the NLDN network. *Allen et al*. [2012] relaxed the constraints by reapportioning monthly observed lightning flashes in each model grid cell using model simulated deep convection precipitation data. At a given time, the simulated LNO_x spatial distribution is a function of model simulated convective precipitation and observed monthly mean flash rate. It is a compromise between the approach by *Kaynak et al*. [2008] and the more self-consistent approach described below.

The other modeling approach prioritizes the self-consistency in the models [e.g., *Wang et al*., 1998b; *Choi et al*., 2005; *Zhao et al*., 2009]. Lightning flash observations are used to generate a lightning flash rate parametrization as functions of simulated convection parameters. One benefit of this approach is that diagnostics of meteorological simulation biases in comparison to the observation can be used directly to infer model biases in simulated flash locations and LNO_x distributions. It is also the necessary approach if lightning flash observations are unavailable or if interactions between weather and chemistry are of interest (e.g., the presence of aerosols affecting the location and strength deep convection).

Another issue that we will examine is if using the postconvection profile, usually taken from cloud-resolving model simulations, is necessary. The current approach is to scale the prescribed postconvection profile to the top of convective cloud, i.e., the shape of the postconvection LNO_x distribution is fixed. When the intensity and mass flux distribution of deep convection change, a self-consistent model should capture the corresponding changes in postconvection LNO_x distributions. The question is if simulated convective transport is adequate to be used in this purpose.

In this work, we will attempt to improve the self-consistency of LNO_x simulations in large-scale 3-D modeling. We will make use of lightning observations and model simulation results to examine if the extensive observation data sets can be applied to define better the correlations of lightning flash rate with a suite of meteorological parameters such that the lightning flash rate parameterization can be improved. We will then examine if the LNO_x vertical distribution profiles derived from the observation based LNOM results are consistent with those previously reported and compare the model simulation results with aircraft observations. The model simulation was carried out for July 2010, a month with significant lightning activity and heavy rainfall over the contiguous U.S. continent. Section 2 describes observation data sets and the models used. Section 3 presents the modeling and analysis results. Conclusions are given in section 4.

2. Observation and Model Descriptions

2.1. Lightning Observations

Cloud-to-ground (CG) lightning flash data from the NLDN are used in this study. The NLDN has over 100 ground-based sensors located across the contiguous United States that detect the characteristic electromagnetic waveform radiated by the return stroke(s) in a CG lightning flash [*Cummins et al*., 1998, http://www.vaisala.com/en/products/thunderstormandlightningdetectionsystems/Pages/NLDN.aspx]. The NLDN also provides information on those flashes that do not strike the Earth's surface, such as intracloud/intercloud (IC) flashes, and that we collectively abbreviate as "IC flashes." Although this study uses the NLDN IC information, note that the NLDN detection efficiency for IC flashes is far less than for CG flashes. This study also obtains information on CG and IC flashes from the Earth Networks Total Lightning Network (ENTLN, http://weather.weatherbug.com/weatherbug-professional/products/total-lightning-network), previously known as the WeatherBug Total Lightning Network. The ENTLN is a global-scale network but has the majority of its sensors covering the contiguous U.S.

The NLDN and ENTLN data, which include the location, time, polarity, and amplitude of each detected flash, provide an observational constraint on the simulated IC/CG ratio (i.e., the ratio of IC to CG count). Figure 1 shows the distributions of observed monthly mean lightning IC and CG flash density measured by NLDN and ENTLN in July 2010. The NLDN IC and CG flash rates are lower than corresponding values from the ENTLN; the reasons are unclear. The correlation coefficient between NLDN and ENTLN data is 0.69 and 0.77 for IC and CG flash densities, respectively. The discrepancies likely reflect the different methodologies used in flash detection and a lower IC detection efficiency of NLDN than ENTLN. The NLDN CG flash detection efficiency is 90–95% within the interior of the U.S., but its IC detection efficiency is very low at 10–20% before the network upgrades in 2013 [*Cummins and Murphy*, 2009]. The ENTLN CG detection efficiency is also $>$90% (S. Heckman, personal communications, 2011), but its IC detection efficiency is higher at ~65% [*Heckman and Liu*, 2010].

For applications of LNO_x estimates, we use the CG flash rates measured by NLDN as in previous studies [e.g., *Allen and Pickering*, 2002; *Ott et al*., 2010]. The CG flash parameterizations to be discussed for section 3.1 are only for the continental region with the detection efficiency corrected NLDN data [*Cummins et al*., 1998]. The same parameterizations are used for coastal regions [*Allen and Pickering*, 2002]. The ENTLN data are used instead as an observational constraint for IC/CG flash rate ratio, which we will compare with the data compiled by *Boccippio et al*. [2001].

Another data set we used in this study is the NALMA data. NALMA is a three-dimensional VHF detection network of 11 VHF receivers deployed across northern Alabama with a base station and receiver located at the National Space Science and Technology Center (http://weather.msfc.nasa.gov/sport/lma/). These data are used to help estimate the LNO_x vertical profile and to evaluate the simulated IC/CG flash rate ratios. More details on the NALMA, including a detailed network error analysis, are included in *Koshak et al*. [2004].

2.2. Weather Research and Forecasting Simulations

The Weather Research and Forecasting (WRF) model is a state of the science nonhydrostatic atmospheric model (http://www.mmm.ucar.edu/wrf/users/pub-doc.html). We use the KF-Eta convection scheme with moist updrafts and downdrafts, including the effects of detrainment and entrainment. Shallow convection is also allowed [*Kain*, 2003]. In the present study, WRF version 3.2.1 was used and was initialized using the assimilated reanalysis data from the National Centers for Environmental Prediction climate forecast System

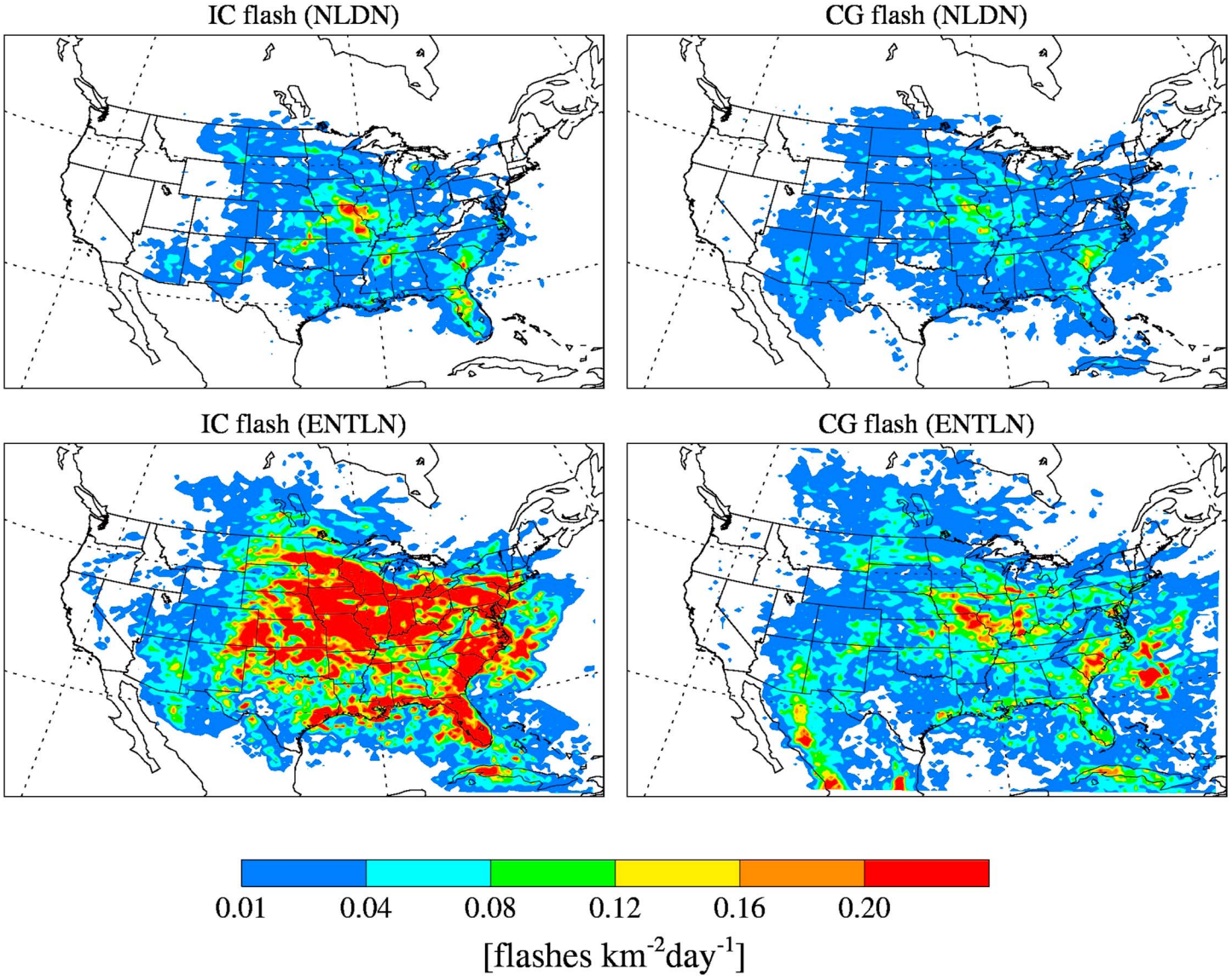

Figure 1. Monthly mean IC and CG flash densities observed by the NLDN and ENTLN networks for July 2010.

Analysis (CFSR) and was run with four-dimensional data assimilation. The WRF Double-Moment 6-class scheme was used for the simulation of microphysics. The domain covers the contiguous United States and part of southern Canada and northern Mexico with a grid spacing of 36 km and 36 vertical layers from the surface to 10 hPa.

2.3. Community Multiscale Air Quality Model Simulations

The Community Multiscale Air Quality (CMAQ) version 4.7 model driven by WRF meteorological data was used in this study. The model has a horizontal resolution of 36 km with 36 vertical layers below 10 hPa. Most meteorological fields are archived every 30 min except those related to convective lightning parameterizations (e.g., CTOP, CAPE, CPR, and UMF). The horizontal domain of WRF has 10 extra grids beyond that of CMAQ model domain on each side to minimize potential transport anomalies near the lateral boundaries. The LNO_x emission calculation described above was updated every 5 min during CMAQ runs. Anthropogenic and biogenic emissions were prepared using the Sparse Matrix Operator Kernel Emissions system [e.g., *Luo et al.*, 2011].

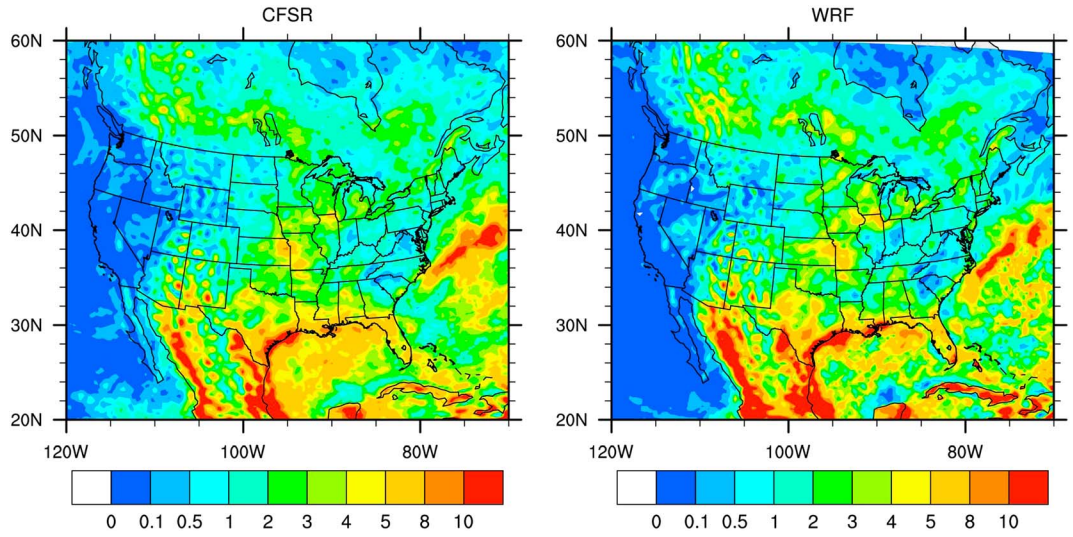

Figure 2. Monthly mean convective precipitation rates (kg m^{-2} d^{-1}) estimated by CFSR reanalysis and WRF simulation for July 2010.

3. Modeling and Analysis Results

To implement LNO_x production consistent with model simulated convection events, we examine which physical parameters best correlate with the observations of CG flash densities. Figure 2 shows that convective precipitation occurred over Missouri, Kansas, the boundary of Illinois, Wisconsin, Florida, and along the coast to the Gulf of Mexico in the CFSR reanalysis data. The WRF simulation reproduces well the reanalysis distribution.

3.1. Relationships of CG Flash Rate With Convection/Cloud Parameters

Correlations of lightning flash densities with convection/cloud parameters were found previously [*Fehr et al.*, 2004; *Choi et al.*, 2005, 2008; *Petersen et al.*, 2005; *Barthe and Barth*, 2008, 2010; *Deierling et al.*, 2008; *McCaul et al.*, 2009; *Zhao et al.*, 2009; *Wong et al.*, 2013; *Finney et al.*, 2014]. In this study, we select the suite of convection/cloud parameters that are available from WRF including ice mass, cloud top height, CAPE, CPR, and UMF [*Price and Rind*, 1993; *Choi et al.*, 2005, 2008; *Deierling and Petersen*, 2008; *Barthe et al.*, 2010].

3.1.1. Cloud Top (CTOP) Height

On the basis of the previous theoretical work by *Vonnegut* [1963] and the analysis by *Williams* [1985], *Price and Rind* [1992] proposed to estimate the lightning flash rate as function of cloud top height:

$$\text{Continental lightning} \qquad f = 3.44\times10^{-5}H^{4.9} \tag{1}$$

$$\text{Marine lightning} \qquad f = 6.2\times10^{-4}H^{1.73}, \tag{2}$$

where f is CG flash rate in flashes per minute and H is cloud top height in kilometer. We estimate CG flash rate distribution in July 2010 using equations (1) and (2). The H value for a given grid column is the altitude at which the convective updraft velocity calculated by the WRF KF-Eta scheme became zero. The flash rate values derived from equations (1) and (2) are then converted to flash densities for use in geographical views; Figure 3 shows the observed CG flash density by the NLDN (top row, left), and the simulated CG flash density derived from CTOP height H using equations (1) and (2) is provided for comparison (top row, middle). Table 1 shows the correlation statistics of correlation coefficient (R), slope of a least squares regression, and mean bias. In general, there is a low bias over parts of northeastern states but a high bias over Georgia, Florida, Alabama. Previously *Barthe et al.* [2010] showed that the flash rate estimated from cloud top height does not reproduce the observed flash density. *Wong et al.* [2013] also evaluated lightning parameterization based on cloud top height [*Price and Rind*, 1992] and showed that the integrated flash count is consistent with the observations, although they needed to add a correction and define CTOP as the height of neutral buoyance —2 km. Our result shows that WRF CTOP estimated CG flash density is of the same order of magnitude as

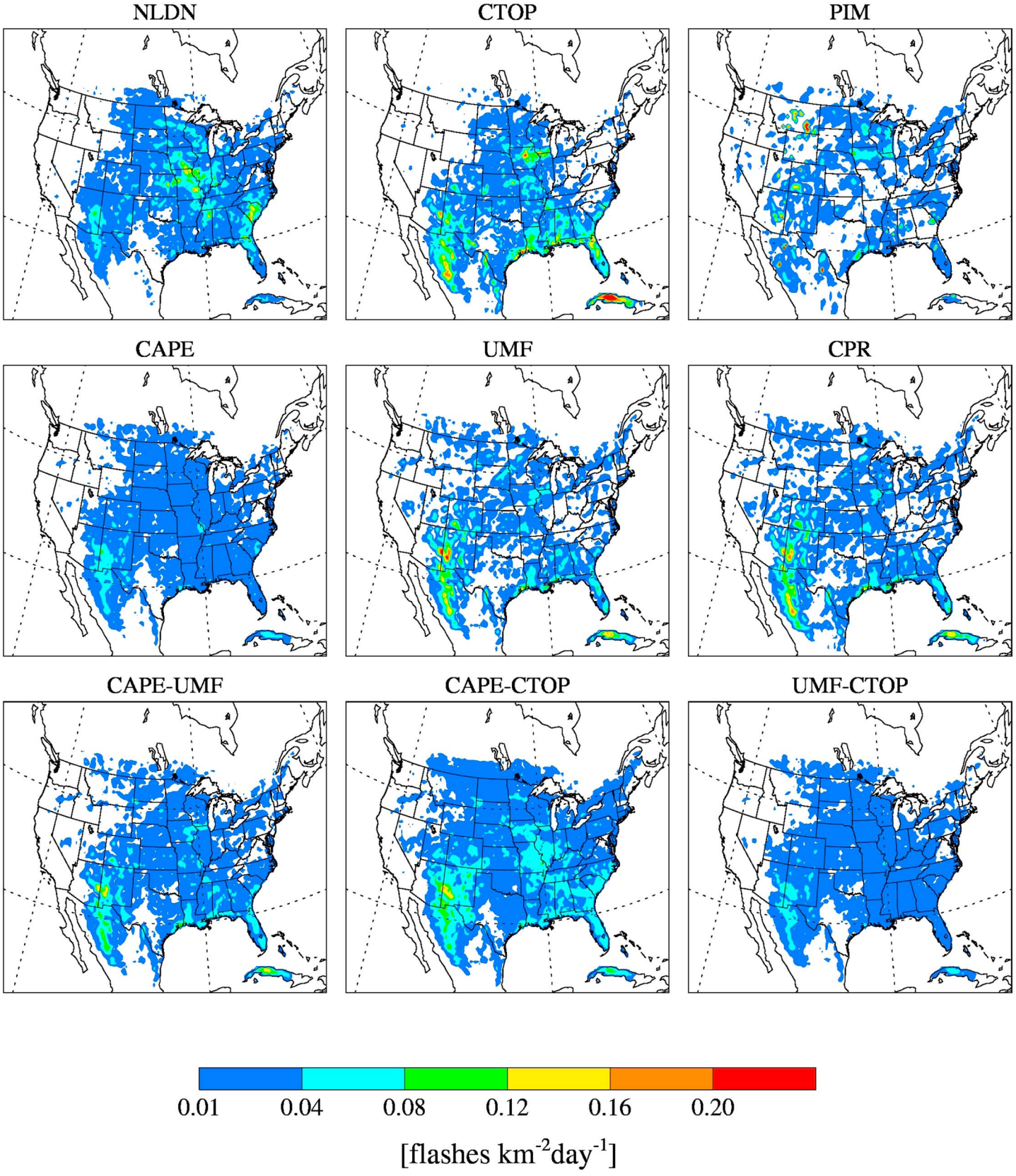

Figure 3. Observed and simulated distribution of monthly mean CG flash density for July 2010. Dependent convection variables used in the parameterizations are listed above the respective panels. See text for the parameterization details.

Table 1. Correlation Statistics of CG Flash Rate[a] With Parameterizations Using Convection Variables

	R	Slope	Relative Bias ((Model - Observed)/Observed)
CTOP	0.52	0.40	−5.6%
PIM	0.25	1.76	−43%
CAPE	0.66	1.16	−8.8%
UMF	0.51	0.48	−25%
CPR	0.39	1.53	−22%
CAPE-UMF[b]	0.69	1.10	−9.5%
CAPE-CTOP[c]	0.75	0.87	−8.3%
UMF-CTOP[d]	0.70	1.26	−19%

[a]The 5 min NLDN CG flash rate observation data and model results are used. There is a total of 6.4×10^6 observed flashes in July 2010.
[b]The coefficients for equation (7) are $a_0=0.80$, $a_1=1.36\times10^{-7}$, $a_2=-2.5\times10^{-3}$, $a_3=3.36$, and $a_4=5.4\times10^{-2}$.
[c]The coefficients for equation (7) are $a_0=7.68$, $a_1=1.23\times10^{-9}$, $a_2=8.32\times10^{-4}$, $a_3=-0.18$, and $a_4=0.45$.
[d]The coefficients for equation (7) are $a_0=5.11$, $a_1=2.42\times10^{-7}$, $a_2=7.91\times10^{-3}$, $a_3=-0.10$, and $a_4=0.90$.

NLDN observations and that the monthly mean simulated flash distribution is reasonable. The correlation coefficient between observed and simulated CG flash density is 0.52. We did not find that adding a correction of −2 km to CTOP values by *Wong et al*. [2013] is necessary. We calculate LNO_x using 5 min CTOP values, whereas *Wong et al*. [2013] used hourly CTOP outputs. The large nonlinear dependence of LNO_x on CTOP (equation (1)) implies that hourly CTOP output introduces biases on LNO_x estimates.

3.1.2. Precipitation Ice Mass

Deierling et al. [2008] analyzed ground-based dual polarimetric radar and total lightning flash data from 11 thunderstorms and obtained a linear relationship between the flash rate and the precipitation ice mass for temperatures less than −5°C:

$$f = 3.4\times10^{-8}P_m - 18.1, \tag{3}$$

where f is CG flash rate in flashes per minute and P_m is precipitation ice mass in kilogram. They obtained a correlation coefficient of 0.94. We estimated flash density using equation (3) and found the correlation (Table 1 and Figure 3) is much lower than *Deierling et al*. [2008]. The poor correlation ($R=0.25$) likely reflects the uncertainties in the model estimate of precipitation ice mass.

3.1.3. Convective Available Potential Energy (CAPE)

CAPE is effectively the positive buoyancy of an air parcel and is an indicator of atmospheric instability, which was used to predict lightning flash frequency by *Choi et al*. [2005] and *Zhao et al*. [2009]. *Choi et al*. [2005] found that the parameterization with CAPE produced a better lightning flash density distribution estimate than that with cloud top height or convective mass flux on the basis of NLDN observations. Here we investigated the relationship between observed flash rate and WRF calculated CAPE using a power law least squares regression. The empirical formula is as follows:

$$f = 1.17E^{0.0069}, \tag{4}$$

where f is CG flash rate in flashes per minute and E is CAPE in J/kg. The simulated monthly mean flash density and correlation statistics are shown in Figure 3 and Table 1, respectively. This method tends to smooth out flash density over the domain and underestimate flash density over very active lightning regions, but nonetheless, the correlation coefficient ($R=0.66$) is relatively high.

3.1.4. Updraft Mass Flux (UMF)

Updraft mass flux intensity can be an indicator of unstable severe weather. More specifically, updraft is a key component of the electrical generator because it drives the development of graupel and ice crystals, enhances particle collision frequencies at updraft boundaries, and together with gravitational force provides a means to separate charge on the cloud scale. *Deierling and Petersen* [2008] suggested that there exists a correlation between total lightning activity and updraft mass flux since the latter affects cloud charge separation. We derive the empirical relationship between flash rate and UMF using a power law least squares regression:

$$f = 0.697\mathrm{UMF}^{0.38}, \tag{5}$$

where f is CG flash rate in flashes per minute and UMF is updraft mass flux in $\mathrm{kg\,m^{-2}\,min^{-1}}$ at 500 hPa. Figure 3 shows that the simulated monthly mean flash density from the UMF parameterization captures high flash activity over Arizona, New Mexico, Florida, south parts of Georgia, and South Carolina but missed flashes over Texas and some parts of northeastern states. Model estimates have high biases over Iowa, Missouri, and Illinois. The correlation coefficient between simulated and observed CG flash rate is about 0.51 (Table 1).

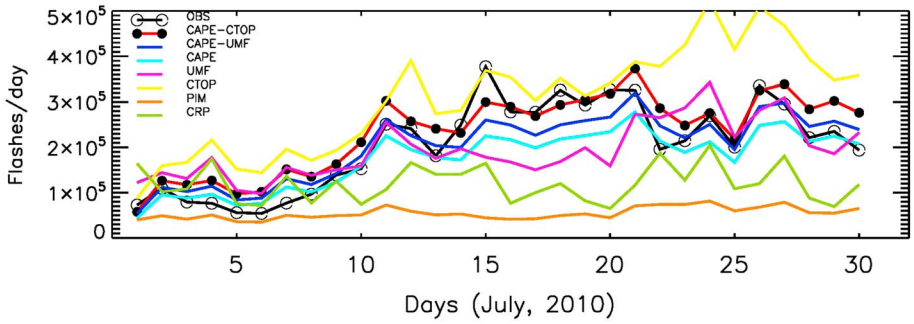

Figure 4. Comparison between simulated and observed total daily flash rates over the contiguous United States for July 2010.

3.1.5. Convective Precipitation Rate (CPR)

We tested the relationship between observed flash rate and convective precipitation rate here by using a gradient-expansion least squares regression. The calculated empirical relationship of observed flash rate and WRF calculated convective rain is as follows:

$$f = 0.537 R_c^{0.12}, \tag{6}$$

where f is CG flash rate in flashes per minute and R_c is model simulated CPR (mm h^{-1}). The correlation coefficient between simulated and observed CG flash density is 0.39, which is lower than all other parameterizations except that using precipitation ice mass (PIM) (Table 1 and Figure 3).

3.1.6. CAPE and CTOP

To further improve the parameterization, we tested NLDN CG flash rate regression using parameter pairs (CAPE and UMF, CAPE and CTOP, and CTOP and UMF). We apply the power law relationship used previously and also include a term for the product of the parameter pair:

$$f = a_0 \cdot x^{a_1} + a_2 \cdot x \cdot y + a_3 \cdot y^{a_4}, \tag{7}$$

where f is CG flash rate in flashes per minute and x and y are the parameters in the same units as in previous formulations. Among the parameter pairs we evaluated, CAPE-CTOP and CAPE-UMF have the best regression statistics (Table 1). The coefficients for equation (7) of the regressions are also given in Table 1.

Figure 3 and Table 1 show that the two-variable parameterization using CAPE-CTOP or CAPE-UMF improves upon the previous single-variable parameterizations. Similar improvements can be seen in the time series of total daily CG flash rate (Figure 4). The general increase from 1 to 15 July, the high flash rate on 15–21 July, the decrease from 21 to 25 July, and the hump-shaped variation on 25–30 July are reproduced better by the two-variable parameterizations than single-variable parameterizations. The parameterization using CAPE and CTOP is better to reproduce the high flash rate on 15–21 July than that using CAPE and UMF. The reasons for the apparent superiority of these variables compared to the others in Table 1 are difficult to diagnose. Inspection of Table 1 indicates that the worst variables to use are PIM and CPR, both of which are affected by microphysics of convective clouds. It appears that the poor correlations using PIM or CPR parameterization are more likely a reflection of deficiency in model microphysics simulation. As model microphysics improves, studies like this one need to be done in order to assess if the related variables offer better predictability of CG flash density. In this study, we use the CAPE-CTOP parameterization to simulate CG flash density in the model.

3.2. Estimating IC Flash Rate

We compute IC flash rate by simply multiplying the CG flash rate with the Z ratio (IC/CG). As in previous studies [*Pickering et al.*, 1998; *Fehr et al.*, 2004; *Zhao et al.*, 2009], we use the parameterization by *Price and Rind* [1992] and compute the Z ratio as a function of the height between the freezing layer and cloud top. To evaluate the model simulation, we use the climatology of the Z ratio for July by *Boccippio et al.* [2001], who combined the observations of the NASA Optical Transient Detector and NLDN. For July 2010, we also have

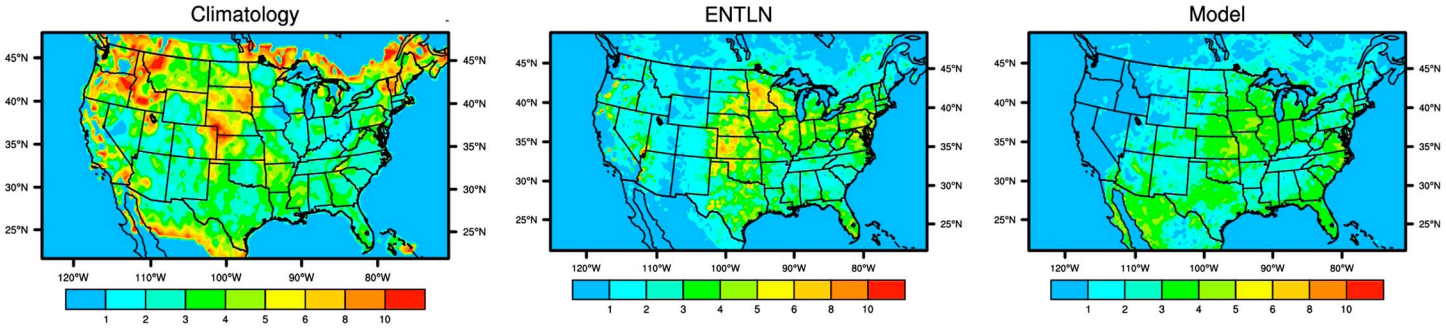

Figure 5. Comparison of simulated *Z* ratio for July 2010 with ENTLN observations and the climatology by *Boccippio et al.* [2001].

observed *Z* ratios from ENTLN. The model estimate is compared to the observations in Figure 5. Over the United States, model estimates show high *Z* ratios (~5) over the central U.S. and Florida as in the ENTLN observation. Since ENTLN observations miss about 1/3 IC flashes [*Heckman and Liu*, 2010], its *Z* ratio has a low bias. The model estimate tends to have an even lower bias. However, the spatial pattern of *Z* ratio distribution is consistent between the model and observations. The climatology by *Boccippio et al.* [2001] shows a similar pattern if we exclude the high *Z* ratio values (~10) over isolated areas in the central U.S. or some regions with infrequent lightning activities.

3.3. Vertical Distribution of LNO_x

In this section, we describe different vertical LNO_x profiles to be used in this study. In order to compare these LNO_x profiles, we must specify the same total LNO_x amount in all simulations. We set a NO_x production rate of 250 mol NO per IC flash and 500 moles per CG flash in this study on the basis of previous studies [*Ott et al.*, 2003; *Choi et al.*, 2005; *Hudman et al.*, 2007; *Zhao et al.*, 2009; *Koshak et al.*, 2014]. The resulting total LNO_x is ~0.14 Tg N over the contiguous U.S. for July 2010.

Simulated LNO_x vertical distribution depends on the initial LNO_x profile [*Pickering et al.*, 1998; *Ott et al.*, 2010; *Koshak et al.*, 2014] and convective transport [*Zhao et al.*, 2009]. A large number of regional and global

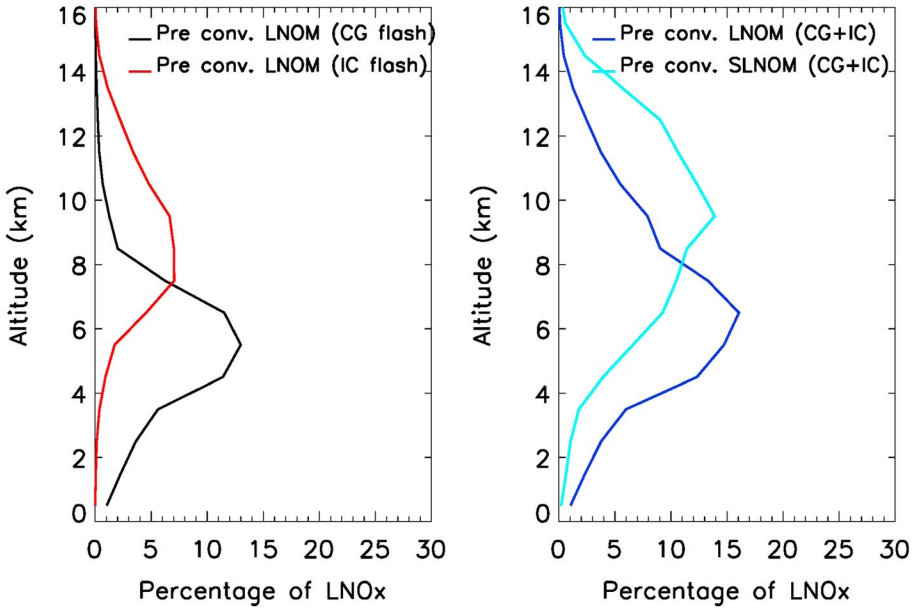

Figure 6. (left) LNOM estimated preconvection IC and CG LNO_x fractional distribution on the basis of NLDN and NALMA observations. (right) Preconvection LNOM and SLNOM LNO_x vertical profiles for July 2010. The LNOM preconvection LNO_x profile in Figure 6 (right) is a summation of IC and CG LNO_x shown in Figure 6 (left). Although LNOM results and LNOM SADs are provided with a vertical resolution of 100 m, the results here have been binned at 1 km vertical resolution.

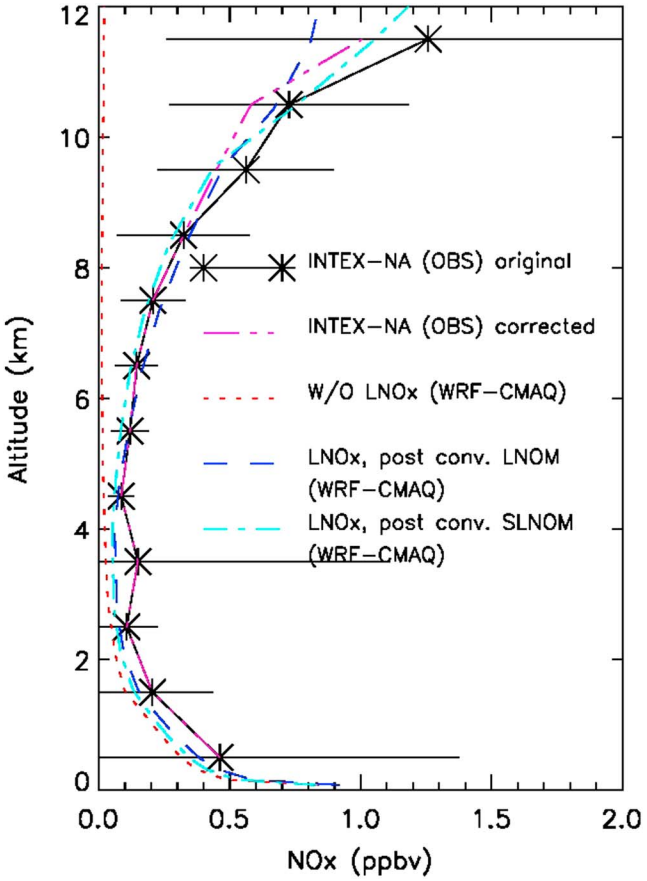

Figure 7. WRF-CMAQ simulated vertical profiles of NO_x with and without LNO_x for July 2010. Postconvection LNOM and SLNOM LNO_x profiles (Figure 6) are used in separate simulations with lightning NO_x. INTEX-NA observed NO_x profile (binned at 1 km interval) in July 2004 and that corrected for upper tropospheric $CH_3O_2NO_2$ interferences ($T < 240$ K, see text) are shown; the asterisk shows the average value, and horizontal bar shows the standard deviation. Daytime (8 A.M. to 6 P.M.) WRF-CMAQ data over the INTEX-NA region (23–55°N and 69–125°W) are shown.

studies used the "C-shaped" LNO_x profile for continental midlatitudes by *Pickering et al.* [1998]. However, the more recent study by *Ott et al.* [2010] suggested a profile update with little LNO_x in the lower atmosphere and increased LNO_x in the middle troposphere.

Koshak et al. [2014] applied the LNOM which ingests NALMA and NLDN data to estimate the LNO_x profile. Hence, the LNOM accounts for the length, altitude, and detailed geometry (tortuosity and branching) of the lightning channel as derived from the NALMA, as well as the observed peak current within the return stroke as derived from the NLDN. The LNOM employs the empirical relations provided in *Wang et al.* [1998a] and *Cooray et al.* [2009] to convert these flash-specific characteristics to LNO_x production (see *Koshak et al.* [2014] for additional details). It is debated as to whether or not CGs produce the same or different amounts of LNO_x compared to ICs [e.g., *Wang et al.*, 1998a; *Ott et al.*, 2010; *Carey et al.*, 2016]. Regarding this debate, one should note that there are four main reasons that the LNOM obtains greater LNO_x production for CGs than ICs:

1. CG channel length is longer on average than IC channel length.
2. CGs have larger currents (more energy) than ICs.
3. CG channel altitude is lower where there are more air molecules to produce more LNO_x.
4. Many CGs have in-cloud components (so called "hybrid flashes") [*Carey et al.*, 2016, and references therein]. Hence, these CGs can be looked at as ICs that additionally have a channel connecting to ground (and this additional channel produces a significant amount of LNO_x [*Koshak et al.*, 2015], particularly since there are typically several return strokes to ground within CGs).

In other words, using the best available parameterizations in the literature, the LNOM computational results show that CGs produce more LNO_x than ICs, on average.

A standard LNOM LNO_x profile, based on lightning observations collected solely from the northern Alabama region, is provided in Figure 6. The LNOM analysis begins by computing the lightning channel segment altitude distribution (SAD) and then applies its various discharge-dependent parameterizations to come up with the LNO_x profile. Note from Figure 6 (left) that since IC flashes occur at higher altitudes, the IC LNO_x production occurs at higher altitudes. IC LNO_x peaks at 7–9 km, while CG LNO_x peaks at 5–7 km. The sum of IC and CG LNO_x (Figure 6, right) shows a peak at 5–8 km, largely resembling that of the CG LNO_x profile. The LNOM LNO_x profiles presented here differ from what is shown in Figure 1 of *Allen et al.* [2012] since the LNOM (including the LNOM-derived SAD) was updated [*Koshak and Peterson*, 2011], and the *Allen et al.* [2012] study employed their own simplified LNO_x parameterization rather than the LNOM LNO_x parameterization.

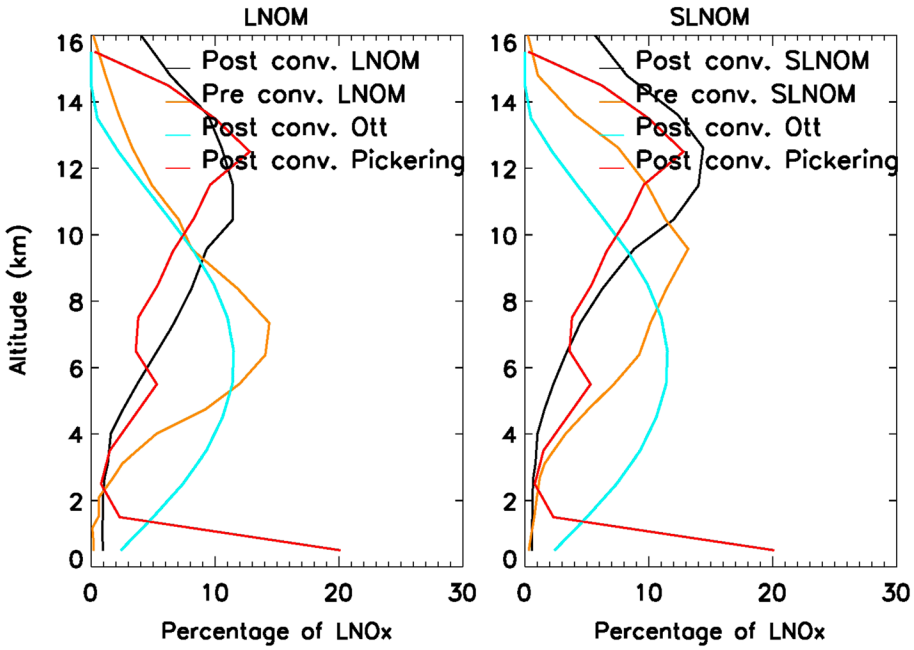

Figure 8. Simulated preconvection and postconvection LNOM and SLNOM fractional distributions of LNO_x in comparison to the postconvection midlatitude profiles by *Pickering et al.* [1998] and *Ott et al.* [2010]. Model data over land of the eastern U.S. (25–50°N and 75–125°W) are binned at 1 km interval.

It is possible to construct an alternate LNO_x profile that employs the same LNOM-derived SAD but that applies to this SAD a simplified LNO_x parameterization that depends only on lightning channel length and air density. We refer to the resulting profile as a "simplified LNOM" (SLNOM) LNO_x profile. Figure 6 compares the standard LNOM LNO_x profile to that of SLNOM. The latter has a broad peak in the upper troposphere with a maximum at around 9 km. We note that the relative proportions of LNO_x distributions shown in Figure 6 (right) are LNO_x profiles that we will apply in the WRF-CMAQ model simulations.

In modeling applications, the postconvection profiles by *Pickering et al.* [1998] and *Ott et al.* [2010] are fundamentally different from the standard LNOM and SLNOM preconvection profiles. The former two postconvection profiles already accounted for convective transport of LNO_x in clouds, while the LNOM and SLNOM preconvection LNO_x profiles in Figure 6, by design, do not. In model implementation, LNO_x emitted using the LNOM or SLNOM profile must be processed by convective mass transport in the model, while care must be taken that LNO_x is not affected by model convections if the other two profiles are used. The benefit of using the LNOM or SLNOM preconvection LNO_x profile is that the redistribution of LNO_x is dependent on model simulated convective transport.

We assess the effect of LNOM and SLNOM preconvection LNO_x profiles on the simulated NO_x distribution. Since in situ observations are unavailable for July 2010, we use the observations in July 2004 from the Intercontinental Chemical Transport Experiment-North America (INTEX-NA). Over the INTEX-NA region, model simulations suggest that upper tropospheric NO_x is mainly produced by lightning (Figure 7), in agreement with *Zhao et al.* [2009]. *Nault et al.* [2015] suggested that the presence of $CH_3O_2NO_2$ in the upper troposphere led to signals of NO_x in the instrument and introduced a positive NO_x bias of ~20% at $T < 240$ K (initially estimated by *Browne et al.* [2011]) for air masses affected by deep convection and lightning. We also show a bias-corrected NO_x profile for the upper troposphere (above 8 km) in Figure 7. In general, the postconvection NO_x vertical distributions using LNOM and SLNOM preconvection LNO_x profiles are very similar, showing an increase with altitude up to 12 km as observed. The SLNOM LNO_x profile leads to higher NO_x above 10 km but lower NO_x at 6–9 km compared to the simulations using the LNOM LNO_x profile. Considering the uncertainties in the measurements and model simulations, the simulated NO_x distributions with LNOM and SLNOM preconvection LNO_x profiles are both in reasonably good agreement with the observations. One further consideration is that the LNOM preconvection LNO_x profile is based on the observations

of NLDN and NALMA. The NALMA observation location has a Z ratio that is lower than other active lightning regions (Figure 5), likely leading to a low-altitude bias in LNO_x when we apply this profile to the contiguous U.S. in the model.

In order to understand better the characteristics of LNO_x simulations, we compare in Figure 8 preconvection and postconvection profiles of LNOM and SLNOM in the context of the postconvection profiles by *Pickering et al*. [1998] and *Ott et al*. [2010]. When applying a preconvection lightning NO_x profile in WRF-CMAQ simulations, we assume that the relative LNO_x distribution from the surface to the top of the convection follows the same proportional shape of that shown in Figure 6 (right). Since the top of the convection is defined by convective mass flux distribution and is not a constant, the averaged preconvection LNOM and SLNOM LNO_x profiles shown here are slightly different from those in Figure 6. The change from preconvection to postconvection LNO_x profiles is drastic. The difference of preconvection LNOM and SLNOM profiles is much reduced after convection. Convective redistribution is a more important factor than preconvection LNO_x profile selection. It is interesting to note that the preconvection LNOM profile is similar to the postconvection profile by *Ott et al*. [2010] and that the postconvection LNOM or SLNOM profile is similar to the postconvection profile by *Pickering et al*. [1998]. The main difference of the latter profiles is that WRF-CMAQ simulated postconvection profiles do not have the increase of LNO_x near the surface, which is in agreement with *Ott et al*. [2010].

4. Conclusions

Advances in analyzing NLDN/NALMA lightning observations with the LNOM make it possible to obtain preconvection LNO_x profiles. With the improvements in the simulation of convective transport by the current generation regional-scale WRF model [*Zhao et al*., 2009], we show in this study that it is now feasible to implement a self-consistent LNO_x scheme in large-scale 3-D models. On the basis of our analysis results, the main conclusions are the following:

1. In the parameterization of CG flash rate, dynamical variables in general offer better simulations than microphysical or precipitation variables. As the microphysics improves in the mesoscale meteorological model, evaluations in section 3.1 need to be carried out to assess if better CG parameterization can be obtained using simulated microphysics variables. At present, we recommend using CAPE and CTOP (equation (7) and Table 1).
2. The Z ratio parameterization by *Price and Rind* [1992] appears to introduce a low bias. However, the spatial distribution is in agreement with ENTLN observations. We note that it is not directly used in LNO_x simulations in our LNO_x scheme. Together with the assumptions for LNO_x per flash rates, which we specified as 250 and 500 mol per flash for IC and CG flashes, respectively, these parameters and the estimated or observed CG flash rate in a given grid cell determine LNO_x column emission rate. In other words, different sets of IC and CG LNO_x per flash rates and Z ratio parameterization (or assumption) can result in the same LNO_x emission rate.
3. Coupled with the WRF KF-Eta convection scheme, the difference of using either the LNOM or SLNOM (preconvection) LNO_x profile is reasonably small in light of the uncertainties in LNO_x parameterizations and observation constraints. While the physical understanding embodied in LNOM will in the future enable better LNO_x profile estimation as our understanding of lightning processes, lightning observation capability, and modeling capability improve, convective redistribution appears to be a more important factor than preconvection LNO_x profile selection, providing another reason for linking the strength of convective transport to LNO_x distribution.
4. It is difficult to use atmospheric observations of NO_x in the convective outflow region to independently determine the per flash IC or CG LNO_x emission rate since it is a combination of preconvection IC and CG LNO_x emissions and convective transport that controls the postconvection LNO_x concentrations.

The LNO_x parameterization scheme and recommendations we presented here are generic. The adaptation of the parameterization scheme into other 3-D models or specific intensive observation periods will likely require changes, and detailed model evaluations will be needed. More in-depth analyses using ground-based LMA, NLDN, and ENTLN measurements, satellite lightning observations, and in situ and remote sensing NO_x data are required to further optimize the parameterizations and improve LNO_x simulations in regional and global models.

Acknowledgments
This work was supported by the NASA Atmospheric Chemistry Modeling and Analysis Program. W.J.K. was also supported by the NASA Program of Climate Indicators and Data Products for Future National Climate Assessments. We are grateful to Stan Heckman, who kindly provided ENTLN data used in this study. Lightning and model data in this study can be found at http://apollo.eas.gatech.edu/data/lightning. The INTEX-NA data are available at https://eosweb.larc.nasa.gov/project/intex-a/intex-a_table.

References

Allen, D. J., and K. E. Pickering (2002), Evaluation of lightning flash rate parameterizations for use in a global chemical transport model, *J. Geophys. Res.*, *107*(D23), 4711, doi:10.1029/2002JD002066.

Allen, D. J., K. E. Pickering, G. Stenchikov, A. Thompson, and Y. Kondo (2000), A three-dimensional total odd nitrogen (NO_y) simulation during SONEX using a stretched-grid chemical transport model, *J. Geophys. Res.*, *105*, 3851–3876, doi:10.1029/1999JD901029.

Allen, D. J., K. E. Pickering, R. W. Pinder, B. H. Henderson, K. W. Appel, and A. Prados (2012), Impact of lightning-NO on eastern United States photochemistry during the summer of 2006 as determined using the CMAQ model, *Atmos. Chem. Phys.*, *12*, 1737–1758, doi:10.5194/acp-12-1737-2012.

Barthe, C., and M. C. Barth (2008), Evaluation of a new lightning-produced NO_x parameterization for cloud resolving models and its associated uncertainties, *Atmos. Chem. Phys.*, *8*, 4691–4710.

Barthe, C., W. Deierling, and M. C. Barth (2010), Estimation of total lightning from various storm parameters: A cloud resolving model study, *J. Geophys. Res.*, *115*, D24202, doi:10.1029/2010JD014405.

Boccippio, D. J., K. L. Cummins, H. J. Christian, and S. J. Goodman (2001), Combined satellite- and surface-based estimation of the intracloud-cloud-to-ground lightning ratio over the continental United States, *Mon. Weather Rev.*, *129*, 108–122.

Browne, E. C., et al. (2011), Global and regional effects of the photochemistry of $CH_3O_2NO_2$: Evidence from ARCTAS, *Atmos. Chem. Phys.*, *11*, 4209–4219, doi:10.5194/acp-11-4209-2011.

Carey, L. D., and S. A. Rutledge (1996), A multiparameter radar case study of the microphysical and kinematic evolution of a lightning producing storm, *J. Meteorol. Atmos. Phys.*, *59*, 33–64.

Carey, L. D., W. Koshak, H. Peterson, and R. M. Mecikalski (2016), The kinematic and microphysical control of lightning rate, extent, and NO_x production, *J. Geophys. Res. Atmos.*, *121*, 7975–7989, doi:10.1002/2015JD024703.

Choi, Y., Y. Wang, T. Zeng, R. V. Martin, T. P. Kurosu, and K. Chance (2005), Evidence of lightning NO_x and convective transport of pollutants in satellite observations over North America, *Geophys. Res. Lett.*, *32*, L02805, doi:10.1029/2004GL021436.

Choi, Y., Y. Wang, T. Zeng, D. Cunnold, E.-S. Yang, R. Martin, K. Chance, V. Thouret, and E. Edgerton (2008), Springtime transitions of O_3, NO_2, and CO over North America: Model evaluation and analysis, *J. Geophys. Res.*, *113*, D20311, doi:10.1029/2007JD009632.

Cooray, V., M. Rahman, and V. Rakov (2009), On the NO_x production by laboratory electrical discharges and lightning, *J. Sol. Atmos. Terr. Phys.*, *71*, 1877–1889, doi:10.1016/j.jastp.2009.07.009.

Cummins, K., and M. J. Murphy (2009), An overview of lightning locating systems: History, techniques, and data uses, with an in-depth look at the U.S. NLDN, *IEEE Trans. Electromagn. Compat.*, *51*(3).

Cummins, K., E. P. Krider, and M. D. Malone (1998), The U.S. National Lightning Detection Network™ and applications of cloud-to-ground lightning data by electric power utilities, *IEEE Trans. Electromagn. Compat.*, *40*(4), 465–480.

Deierling, W., and W. A. Petersen (2008), Total lightning activity as an indicator of updraft characteristics, *J. Geophys. Res.*, *113*, D16210, doi:10.1029/2007JD009598.

Deierling, W., W. A. Petersen, J. Latham, S. Ellis, and H. J. Christian (2008), The relationship between lightning activity and ice fluxes in thunderstorms, *J. Geophys. Res.*, *113*, D15210, doi:10.1029/2007JD009700.

Dye, J. E., J. J. Jones, A. J. Weinheimer, and W. P. Winn (1989), Observations within two regions of charge during initial thunderstorm electrification, *Q. J. R. Meteorol. Soc.*, *114*(483), 1271–1290.

Fehr, T., H. Höller, and H. Huntrieser (2004), Model study on production and transport of lightning-produced NO_x in a EULINOX supercell storm, *J. Geophys. Res.*, *109*, D09102, doi:10.1029/2003JD003935.

Finney, D. L., R. M. Doherty, O. Wild, H. Huntrieser, H. C. Pumphrey, and A. M. Blyth (2014), Using cloud ice flux to parametrise large-scale lightning, *Atmos. Chem. Phys.*, *14*, 1266512682, doi:10.5194/acp-14-12665-2014.

Heckman, S., and C. Liu (2010), The application of total lightning detection and cell tracking for severe weather prediction, in *International Conference on Grounding and Earthing 2010 and the 4th International Conference on Lightning Physics and Effects*, pp. 234–240, SBRAI, Salvador, Brazil.

Hudman, R. C., et al. (2007), Surface and lightning sources of nitrogen oxides over the United States: Magnitudes, chemical evolution, and outflow, *J. Geophys. Res.*, *112*, D12S05, doi:10.1029/2006JD007912.

Kain, J. S. (2003), The Kain-Fritsch convective parameterization: An update, *J. Appl. Meteorol.*, *43*, 170–181, doi:10.1175/1520-0450(2004)043.

Kaynak, B., Y. Hu, R. V. Martin, A. G. Russell, Y. Choi, and Y. Wang (2008), The effect of lightning NO_x production on surface ozone in the continental United States, *Atmos. Chem. Phys.*, *8*, 5151–5159.

Koshak, W., and H. Peterson (2011), A summary of the NASA Lightning Nitrogen Oxides Model (LNOM) and recent results, 10th Annual CMAS Conference, Chapel Hill, NC.

Koshak, W. J., et al. (2004), North Alabama Lightning Mapping Array (LMA): VHF source retrieval algorithm and error analyses, *J. Atmos. Oceanic Technol.*, *21*, 543–558.

Koshak, W. J., R. J. Solakiewicz, and H. S. Peterson (2015), A return stroke NO_x production model, *J. Atmos. Sci.*, *72*(2), 943–954.

Koshak, W., H. Peterson, A. Biazar, M. Khan, and L. Wang (2014), The NASA Lightning Nitrogen Oxides Model (LNOM): Application to air quality modeling, *Atmos. Res.*, 363–369.

Labrador, L. J., R. von Kuhlmann, and M. G. Lawrence (2004), Strong sensitivity of the global mean OH concentration and the tropospheric oxidizing efficiency to the source of NO_x from lightning, *Geophys. Res. Lett.*, *31*, L06102, doi:10.1029/2003GL019229.

Lamarque, J.-F., G. P. Brasseur, P. G. Hess, and J.-F. Müller (1996), Three-dimensional study of the relative contributions of the different nitrogen sources in the troposphere, *J. Geophys. Res.*, *101*, 22,955–22,968, doi:10.1029/96JD02160.

Luo, C., Y. Wang, S. Mueller, and E. Knipping (2011), Diagnosis of an underestimation of summertime sulfate using the Community Multiscale Air Quality model, *Atmos. Environ.*, *45*, 5119–5130, doi:10.1016/j.atmosenv.2011.06.029.

Martini, M., D. J. Allen, K. E. Pickering, G. L. Stenchikov, A. Richter, E. J. Hyer, and C. P. Loughner (2011), The impact of North American anthropogenic emissions and lightning on long-range transport of trace gases and their export from the continent during summers 2002 and 2004, *J. Geophys. Res.*, *116*, D07305, doi:10.1029/2010JD014305.

McCaul, E. W., S. J. Goodman, K. M. LaCasse, and D. J. Cecil (2009), Forecasting lightning threat using cloud-resolving model simulations, *Weather Forecasting*, *24*, 709–729.

Nault, B. A., C. Garland, S. E. Pusede, P. J. Wooldridge, K. Ullmann, S. R. Hall, and R. C. Cohen (2015), Measurements of $CH_3O_2NO_2$ in the upper troposphere, *Atmos. Meas. Tech.*, *8*, 987–997, doi:10.5194/amt-8-987-2015.

Ott, L. E., K. Pickering, G. Stenchikov, R. Lin, B. Ridley, J. Lopez, M. Loewenstain, and E. Richard (2003), Trace gas transport and lightning NO_x production during a CRYSTAL-FACE thunderstorm simulated using a 3-D cloud-scale chemical transport model, *Eos Trans. AGU*, *84*(46), Fall Meet. Suppl., Abstract AE32A-0156.

Ott, L. E., K. E. Pickering, G. L. Stenchikov, D. J. Allen, A. J. DeCaria, B. Ridley, R.-F. Lin, S. Lang, and W.-K. Tao (2010), Production of lightning NO_x and its vertical distribution calculated from three-dimensional cloud-scale chemical transport model simulations, *J. Geophys. Res.*, *115*, D04301, doi:10.1029/2009JD011880.

Petersen, W. A., S. A. Rutledge, and R. E. Orville (1996), Cloud-to-ground lightning observations to TOGA COARE, selected results and lightning location algorithm, *Mon. Weather Rev.*, *124*(4), 602–620.

Petersen, W. A., S. A. Rutledge, R. C. Cifelli, B. S. Ferrier, and B. F. Smull (1999), Shipborne Dual-Doppler operations during TOGA COARE: Integrated observations of storm kinematics and electrification, *Bull. Am. Meteorol. Soc.*, *80*(1), 81–96.

Petersen, W. A., H. J. Christian, and S. A. Rutledge (2005), TRMM observations of the global relationship between ice water content and lightning, *Geophys. Res. Lett.*, *32*, L14819, doi:10.1029/2005GL023236.

Pickering, K. E., Y. Wang, W.-K. Tao, C. Price, and J.-F. Muller (1998), Vertical distributions of lightning NO_x for use in regional and global chemical transport models, *J. Geophys. Res.*, *103*, 31,203–31,216, doi:10.1029/98JD02651.

Price, C., and D. Rind (1992), A simple lightning parameterization for calculating global lightning distributions, *J. Geophys. Res.*, *97*, 9919–9933, doi:10.1029/92JD00719.

Price, C., and D. Rind (1993), What determines the cloud-to-ground lightning fraction in thunderstorms?, *Geophys. Res. Lett.*, *20*, 463–466, doi:10.1029/93GL00226.

Rutledge, S. A., E. R. Williams, and T. D. Keenan (1992), The down under Doppler and electricity experiment (DUNDEE): Overview and preliminary results, *Bull. Am. Meteorol. Soc.*, *73*(1), 3–16.

Schumann, U., and H. Huntrieser (2007), The global lightning-induced nitrogen oxides source, *Atmos. Chem. Phys.*, *7*, 3823–3907, doi:10.5194/acp-7-3823-2007.

Stockwell, D. Z., C. Giannakopoulos, P.-H. Plantevin, G. D. Carver, M. P. Chipperfield, K. S. Law, J. A. Pyle, D. E. Shallcross, and K.-Y. Wang (1999), Modelling NO_x from lightning and its impact on global chemical fields, *Atmos. Environ.*, *33*, 4477–4493, doi:10.1016/S1352-2310(99)00190-9.

Tost, H., P. Jöckel, and J. Lelieveld (2007), Lightning and convection parameterisations—Uncertainties in global modelling, *Atmos. Chem. Phys.*, *7*, 4553–4568, doi:10.5194/acp-74553-2007.

Vonnegut, B. (1963), Some facts and speculations concerning the origin and role of thunderstorm electricity, *Meteorol. Monogr.*, *5*, 224–241.

Wang, Y., A. W. DeSilva, G. C. Goldenbaum, and R. R. Dickerson (1998a), Nitric oxide production by simulated lightning: Dependence on current, energy, and pressure, *J. Geophys. Res.*, *103*(D15), 19,149–19,159, doi:10.1029/98JD01356.

Wang, Y., D. J. Jacob, and J. A. Logan (1998b), Global simulation of tropospheric O_3-NO_x-hydrocarbon chemistry, 1. Model formulation, *J. Geophys. Res.*, *103*, 10,713–10,725, doi:10.1029/98JD00158.

Williams, E. R., and R. M. Lhermitte (1983), Radar tests of the precipitation hypothesis for thunderstorm electrification, *J. Geophys. Res.*, *88*, 10,984–10,992, doi:10.1029/JC088iC15p10984.

Williams, E. R. (1985), Large scale charge separation in thunderclouds, *J. Geophys. Res.*, *90*(D4), 6013–6025, doi:10.1029/JD090iD04p0601.

Wong, J., M. C. Barth, and D. Noone (2013), Evaluating a lightning parameterization based on cloud-top height for mesoscale numerical model simulations, *Geosci. Model Dev.*, *6*, 429–443, doi:10.5194/gmd-6-429-2013.

Zhao, C., Y. H. Wang, Y. Choi, and T. Zeng (2009), Summertime impact of convective transport and lightning NO_x production over North America: Modeling dependence on meteorological simulations, *Atmos. Chem. Phys.*, *9*, 4315–4327.